*Proceedings of the 6th World Congress on Momentum, Heat and Mass Transfer (MHMT'21)*
*~~Lisbon, Portugal~~ Virtual Conference– June 17 – 19, 2021*
*Paper No. ENFHT 201*
*DOI: 10.11159/enfht21.lx.201*

# Numerical Modelling and Analysis of a Microfluidic PCR Device

**Foteini Zagklavara[1*], Peter K. Jimack[1], Nikil Kapur[1], Osvaldo M. Querin[1], Harvey M. Thompson[1]**
[1]University of Leeds, Woodhouse LS2 9JT, Leeds, UK
fotizagl@hotmail.com; P.K.Jimack@leeds.ac.uk; N.Kapur@leeds.ac.uk; O.M.Querin@leeds.ac.uk;
H.M.Thompson@leeds.ac.uk

***Abstract*** **-** Polymerase Chain Reaction (PCR) is widely used in biological research labs in order to detect hereditary diseases, diagnose infectious diseases, clone genes and other purposes. This work focuses on combining CFD and response surface modelling to explore the dependence of DNA amplification on two design parameters in a single phase, continuous flow PCR microfluidic device, consisting of a serpentine-like rectangular channel with three copper wire heaters. The spacing and the width of the microchannel between the heaters are selected as the two design parameters investigated. COMSOL Multiphysics® 5.4 is used to simulate the performance and function of the microfluidic channel, while Design of Experiments and a polyharmonic spline are used to produce the response surface. The results indicate a ~1.4% increase at the value of [DNA] in one PCR cycle.

***Keywords*****:** Microfluidics, PCR, COMSOL

## 1. Introduction

Since its invention by Kary Mulis in 1983 [1], Polymerase Chain Reaction (PCR) has led to significant advances in biology and diagnostics. PCR describes a reaction, where a very small DNA sample is amplified exponentially [2]. In order for the DNA amplification to happen, three distinct stages (denaturation, annealing, extension) need to take place consecutively, for a number of times (PCR cycles). The first of the three stages, denaturation, takes place at ~95 $^{o}$C, where the double-stranded DNA molecules denature into pairs of single-stranded ones. The second stage, annealing, takes place at ~56 $^{o}$C, where the primers form primer-template complexes. The final step of PCR, extension, takes place at ~70 $^{o}$C, where the DNA-polymerase attaches to the primer-template complexes [3].

Several designs of microfluidic devices performing PCR have been published since the invention of PCR [4 - 9]. Even though such devices are widely used, the yield of PCR appears to be affected by adsorption phenomena taking place close to the wall, carryover contamination and varying residence time of the PCR mixture along the cross-section of the channel [10].

These limitations have led to the development of droplet-based μPCR devices (DR-PCR), where droplets carry the DNA sample along the microfluidic device, offering good temperature uniformity due to their small size and a restricted environment, where contamination and adsorption phenomena are less luckily to take place [11, 12, 13, 10]. However, due to the higher cost and complexity of DR-PCR devices [10], a lot of research is taking place on improving the performance, sensitivity and specificity of the single-phase (SP) continuous flow (CF) PCR devices [14]. More specifically, a number of studies can be found on studying the effect that the geometrical parameters or operating conditions can have on the efficiency of PCR [15,16, 17] and simulating the PCR kinetics, heat transfer and fluid flow in such devices [17, 18, 19].

## 2. Problem Description

This work uses COMSOL Multiphysics® 5.4 to simulate the flow, heat transfer and PCR kinetics that take place in a single-phase (SP) continuous flow (CF) μPCR device with a serpentine structure and a rectangular cross-sectional area, similar to the one presented in the work of [19]. Three copper wire heaters are placed at the bottom of the device, creating three distinct temperature zones (95, 55 and 72 $^{o}$C for denaturation, annealing and extension respectively). As the fluid passes through the different temperature zones, the temperature reaches the values required and remains in each zone for a specific amount of time (residence time), needed for PCR to take place [19]. The substrate material (Kapton, PDMS and PE) properties are presented in Table 2 of [19], while the volumetric flow rate is set at $Q_{vol} = 3 \cdot 10^{-11}$ m$^3$/s. The width of the microchannel at the extension zone is twice the size of the other temperature regimes, while the PCR protocol followed in

this work for denaturation, annealing and extension is 3.0s:4.2s:6.2s respectively [19]. Furthermore, the width ($W_{gap}$) and length ($L_{gap}$) of the microchannel between the heaters is optimised, in order to achieve the maximum DNA amplification in one PCR cycle (unitcell, Figure 1). The models of Fluid Flow, Heat Transfer and PCR Kinetics are implemented in COMSOL Multiphysics® 5.4 in steady state [19].

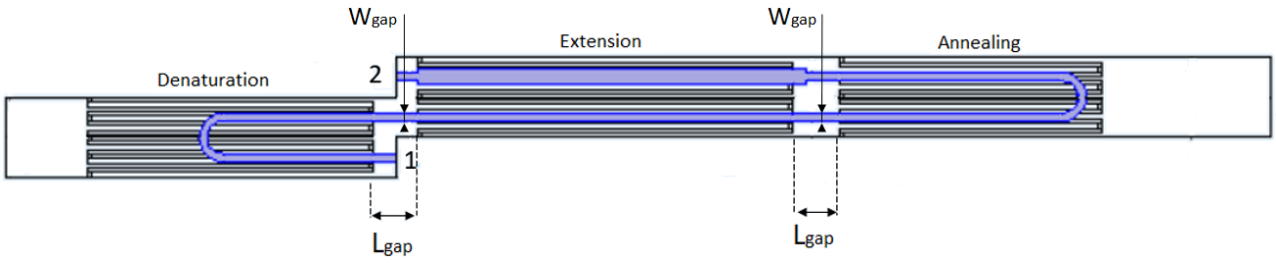


Fig. 1: Schematic graph of unitcell.

### 2.1. Fluid Flow

Navier Stokes equations are used to describe the fluid flow [20] in the microfluidic channel. After testing for the case of 72°C, $Q_{vol} = 3 \cdot 10^{-11}$ m$^3$/s and $W_{gap}$ = 100 μm (for the fluid properties of water [19]), the Reynolds number (Equations 1 and 2) is found equal to 0.35, indicating a laminar flow. A no-slip boundary condition is implemented at the walls of the channel.

$$U = \frac{Q_{vol}}{A} = \frac{Q_{vol}}{(H \cdot W_{gap})} \tag{1}$$

$$\mathrm{Re} = D_h \cdot \mathrm{U} \cdot \frac{\rho}{\mu} = \frac{2H \cdot W_{gap} \cdot U \cdot \rho}{\mu\left(H + W_{gap}\right)} = 0.35 \tag{2}$$

### 2.2. Heat Transfer

The heat transfer model is applied in steady-state (Equation 3) in the entire unitcell. The velocity field (**u**) is only non-zero in the fluid domain. The $\rho C_p(\mathbf{u}\cdot\nabla T)$ and the $\nabla\cdot(k\nabla T)$ terms of Equation 3 describe the convective and conductive heat transfer terms respectively, with the $\rho C_p(\mathbf{u}\cdot\nabla T)$ term being non-zero only in the fluid domain. The second term in the RHS describes the heat generation rate of the j$^{th}$ (j ={1, 2, 3}) heater, and it is only non-zero at the j$^{th}$ heater-kapton interface. The variation in the heat generation rates is implemented in order to achieve the different desired temperatures required for denaturation, annealing and extension (95, 55 and 72 °C respectively). The third term in the RHS of Equation 3 describes the heat flux caused by thermal radiation for each of the solid substrates, i (i ={Copper, PDMS,PE, Kapton}). This term is only non-zero at the outer surfaces of the substrate materials and is given by Equation 4. The $Q_{nat.conv}$ term describes the heat losses to the ambient, as presented in Equation 5:

$$\rho\, C_p(\mathbf{u}\cdot\nabla T) = \nabla\cdot(k\nabla T) + \sum Q_{heater,j} + \sum Q_{rad,i} + Q_{nat.conv.} \tag{3}$$

$$Q_{rad,i} = \varepsilon_i \sigma (T_{amb}^4 - T^4) \tag{4}$$

$$Q_{nat.conv.} = h(T_{amb} - T) \tag{5}$$

Here, $T_{amb}$: the ambient temperature, $\varepsilon_i$: surface emissivity for solid i, $\sigma$: the Stefan–Boltzmann constant and h: the heat transfer coefficient. As far as the boundary conditions are concerned: i) a periodic boundary condition for the temperature is applied at the inlet and outlet of the unitcell, ii) periodic boundary conditions are implemented at the sides of the microchannel, iii) natural convection (Equation 5) and thermal radiation (Equation 4) boundary conditions are applied at the top, bottom, front and back sides of the unitcell for all the different materials [19] and iv) three constant temperature boundary conditions are introduced at the interface between the copper wires and the bottom solid substrate ($T_{den}$ = 95 $^oC$, $T_{ext}$ = 72$^oC$ and $T_{ann}$ = 55 $^oC$) to replace the Joule Heating model used in [19] (apart from Sections 3.1.1 and 3.1.2). This replacement is made in order to avoid the trial and error process required to define the values of the current in each heater, and is expected to lead to greater temperature uniformity and greater values of DNA amplification.

### 2.3. PCR Kinetics

The PCR kinetics, reactions and reaction rate constants used in [19] are introduced in COMSOL Multiphysics 5.4®. The general form of the mass conservation of species in steady state is presented in Equation 6:

$$-\nabla \cdot D_k \nabla C_k + \boldsymbol{u} \cdot \nabla C_k = R_k \tag{6}$$

where $C_k$: the concentration of the $k^{th}$ species (k={1,2,..,7} that correspond to $S_1S_2$ (double-stranded DNA), $S_1$ (single-stranded DNA), $S_2$ (single-stranded DNA), $P_1$ (single-stranded primer molecule), $P_2$ (single-stranded primer molecule), $S_1P_2$ (single-stranded template primer) and $P_1S_2$ (single-stranded template primer) respectively [19], $R_k$: the reaction rate of the $k^{th}$ species, $D_k$: the diffusion coefficient of the $k^{th}$ species. As far as the boundary conditions are concerned, a zero-flux boundary condition is implemented at the walls of the microfluidic channel. The inlet concentrations of the seven species can be found at Table 3 of [19], together with the diffusion coefficients of Equations 6.

## 3. Methodology

### 3.1. Computational Model

The model described in Sections 2.1, 2.2 and 2.3 is implemented in COMSOL Multiphysics 5.4®, using the Laminar Flow, Heat Transfer in Solids and Fluids and Transport of Diluted Species Physics models respectively in steady state. Section 3.1.1 presents the mesh independence study performed while section 3.1.2 presents the validation of the model with the work of [19]. The Joule Heating model is used in both Sections 3.1.1 and 3.1.2 [19]. Section 3.2 describes the method used to generate the response surface of the DNA amplification.

#### 3.1.1. Mesh Independence Study

After generating the model of the unitcell, a mesh independence study is completed in order to ensure both convergence and independence of the solution from the mesh resolution. Five meshes are generated using the physics controlled mesh selection in COMSOL Multiphysics 5.4®; normal (~164,000 elements), fine (~321,000 elements), finer (~866,000 elements), extra fine (~4,036,000 elements) and extremely fine (~6,133,000 elements). The values of $log_2 \frac{[\mathrm{DNA}]}{[\mathrm{DNA}]_o}$ (where [DNA] is the DNA concentration at the end of the channel and $[DNA]_o$ the initial DNA concentration) and energy consumption, $P_h$, for all meshes are found to be equal to 0.67 and 0.071 W respectively. The values of unitcell pressure drop ($\Delta$P(Pa)) are also collected and found to be equal to 288.59, 284.29, 283.05, 286.01, 285.98 for normal, fine, finer, extra fine and extremely fine meshes respectively. As a result, the ~321,000 elements mesh is selected since it presents an acceptable deviation from the finest mesh for the pressure drop.

#### 3.1.2. Validation of the Model

After implementing the model described in Section 2, the results are validated with the ones presented by [19]. Firstly, the value of $log_2 \frac{[\mathrm{DNA}]}{[\mathrm{DNA}]_o}$ (measurement of DNA amplification) is found to be equal to the value of 0.67 presented by [19].

The value of power required or performing one PCR cycle is also found to be 0.071 W, equal to the one presented in the work of [19].

### 3.2. Response Surface Modelling

After completing the mesh independence study and validation of the model, the response surface of $log_2 \frac{[DNA]}{[DNA]_o}$ is generated. More specifically, the spacing ($L_{gap}$) and width ($W_{gap}$) of the microchannel between the three heaters of the SP-CF PCR device (Figure 1) are chosen as the two design parameters to be investigated, with the design domain varying from 500 - 2500 μm and 100 - 200 μm respectively. The dependence of $log_2 \frac{[DNA]}{[DNA]_o}$ (the measurement of the DNA amplification) on $L_{gap}$ and $W_{gap}$ is presented in Figure 2.

#### 3.2.1. Design of Experiments

In order to investigate the behaviour of $log_2 \frac{[DNA]}{[DNA]_o}$ over the design domain, 80 Design of Experiments (DoE) simulations are run. The DoE points are generated using Morris Michel Latin Hypercubes [21, 22] and include the corner points of the design domain.

#### 3.2.2. Response Surface

After performing the simulations in all DoE points, the values of $log_2 \frac{[DNA]}{[DNA]_o}$ are collected. These values are then scaled between zero and one. The response surface of $log_2 \frac{[DNA]}{[DNA]_o}$ is generated, using a third order polyharmonic spline [23] (Figure 2).

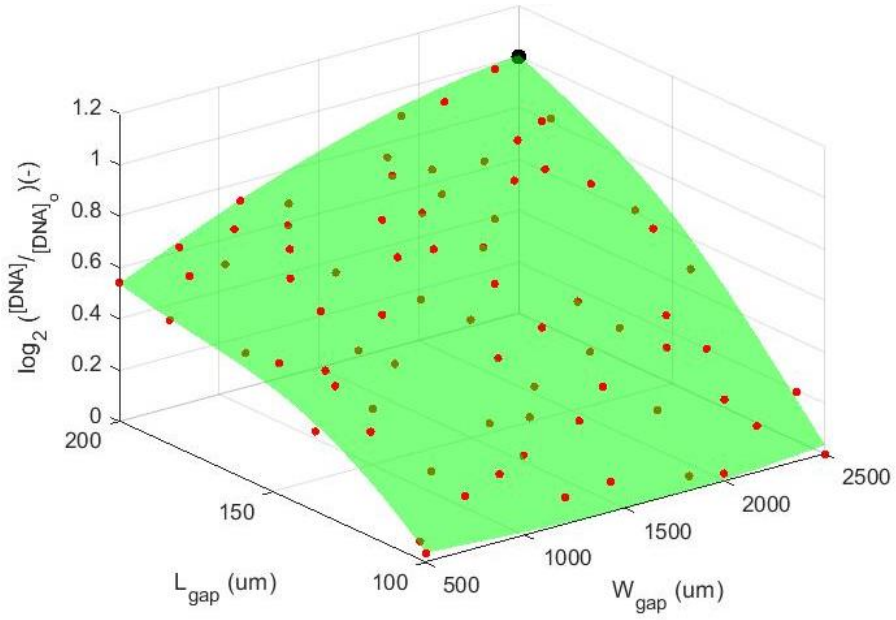


Fig. 2: Response surface of $\log_2 \frac{[DNA]}{[DNA]_o}$. The optimum design is presented in black.

## 3. Results

The response surface of $log_2 \frac{[\mathrm{DNA}]}{[\mathrm{DNA}]_o}$ is presented in Figure 2, while the best design solution ($[W_{gap}, L_{gap}]_{opt}$ = [200 μm, μm, 2500 μm]) is presented in black. The results indicate that by increasing the spacing of the heaters, 3% increase in the the value of $log_2 \frac{[\mathrm{DNA}]}{[\mathrm{DNA}]_o}$ (or ~ 1.4% in the value of [DNA]) can be achieved. Considering these results, future work is expected expected to focus on examining different design variables for further optimisation of the unitcell's performance.

## 4. Conclusion

According to the results obtained from this work, one can observe that by improving the original design [19] to ($[W_{gap}, L_{gap}]_{opt}$ = [200 μm, 2500 μm]), a 3% increase in the value of $log_2 \frac{[\mathrm{DNA}]}{[\mathrm{DNA}]_o}$ (or ~ 1.4% in the value of [DNA]) can be achieved. Further examination of other design parameters of the device is expected to achieve an even greater improvement at the DNA amplification. Furthermore, future work is expected to focus on studying the DNA amplification in a sequence of unitcells, while also considering other objective functions, such as the pressure drop.


## Acknowledgements

The funding of this project is received from EPSRC [24].


## References


[1] K. B. Mullis, "The unusual origin of the polymerase chain reaction, "Scientific American, vol. 262, no. 4, pp. 56–65, 1990.

[2] M. T. Rahman, M. S. Uddin, R. Sultana, A. Moue, and M. Setu, "Polymerase chain reaction (pcr): a short review,"Anwer Khan Modern Medical College Journal, vol. 4, no. 1, pp. 30–36, 2013.

[3] J. Park and H. Park, "Thermal cycling characteristics of a 3d-printed serpentine microchannel for dna amplification by polymerase chain reaction, "Sensors and Actuators A: Physical, vol. 268, pp. 183–187, 2017.

[4] Y. S. Shin, K. Cho, S. H. Lim, S. Chung, S.-J. Park, C. Chung, D.-C. Han, and J. K. Chang, "Pdms-based micro pcr chip with parylene coating, "Journal of Micromechanics and Microengineering, vol. 13, no. 5, p. 768,2003.

[5] A. F. Sauer-Budge, P. Mirer, A. Chatterjee, C. M. Klapperich, D. Char-gin, and A. Sharon, "Low cost and manufacturable complete microtas for detecting bacteria, "Lab on a Chip, vol. 9, no. 19, pp. 2803–2810, 2009.

[6] A. K. Yetisen and L. R. Volpatti, "Patent protection and licensing in microfluidics, "Lab on a Chip, vol. 14, no. 13, pp. 2217–2225, 2014.

[7] S. W. Kim and K. Mi-Ree, "High-speed real-time pcr device based on lab-on-a-chip for detecting food-borne bacteria to agrifood, and methods for detecting food-borne bacteria to agrifood using the same," Apr. 2 2019, uS Patent 10,245,590.

[8] M. Le Berre, "Microfluidic sample chip, assay system using such a chip, and pcr method for detecting dna sequences," Dec. 26 2019, uS Patent App.16/471,500.

[9] M. Le Berre, A. Plecis, and W. Minnella, "Thermalizing microfluidic chip employing variable temperature cycles, system using such a chip and pcr method for detecting dna sequences," Jan. 16 2020, uS Patent App.16/471,517.

[10] Y. Zhang and H.-R. Jiang, "A review on continuous-flow microfluidic pcr in droplets: Advances, challenges and future, "Analytica chimica acta, vol.914, pp. 7–16, 2016.

[11] S.-Y. Ma, Y.-C. Chiang, C.-H. Hsu, J.-J. Chen, C.-C. Hsu, A.-C. Chao, and Y.-S. Lin, "Peanut detection using droplet microfluidic polymerase chain reaction device, "Journal of Sensors, vol. 2019, 2019.

[12] W. Wang, Z.-X. Li, R. Luo, S.-H. L¨u, A.-D. Xu, and Y.-J. Yang, "Droplet-based micro oscillating-flow pcr chip, "Journal of Micromechanics and Microengineering, vol. 15, no. 8, p. 1369, 2005.

[13] J. Shi, S. Xiang, and X. Song, "Droplet digital pcr chip," Jan. 2 2020, uS Patent App. 16/465,438.

[14] S. Yang and R. E. Rothman, "Pcr-based diagnostics for infectious diseases: uses, limitations, and future applications in acute-care settings, "The Lancet infectious diseases, vol. 4, no. 6, pp. 337–348, 2004.

[15] S. Thomas, R. L. Orozco, and T. Ameel, “Thermal gradient continuous-flow pcr: a guide to design, ”Microfluidics and nanofluidics, vol. 17, no. 6,pp. 1039–1051, 2014.
[16] J. J. Chen, C. M. Shen, and Y. W. Ko, “Analytical study of a microfluidic dna amplification chip using water cooling effect, ”Biomedical microdevices, vol. 15, no. 2, pp. 261–278, 2013.
[17] Q. Cao, M.-C. Kim, and C. Klapperich, “Plastic microfluidic chip for continuous-flow polymerase chain reaction: Simulations and experiments, ”Biotechnology journal, vol. 6, no. 2, pp. 177–184, 2011.
[18] L. Wang and P. C. Li, “Optimization of a microfluidic microarray device for the fast discrimination of fungal pathogenic dna,”Analytical biochemistry, vol. 400, no. 2, pp. 282–288, 2010.
[19] V. E. Papadopoulos, G. Kokkoris, I. N. Kefala, and A. Tserepi, “Comparison of continuous-flow and static-chamber μpcr devices through a computational study: the potential of flexible polymeric substrates, ”Microfluidics and Nanofluidics, vol. 19, no. 4, pp. 867–882, 2015.
[20] Y. Wang, “Solving incompressible navier-stokes equations on heterogeneous parallel architectures,” Ph.D. dissertation, 2015.
[21] M. D. Morris and T. J. Mitchell, “Exploratory designs for computational experiments, ”Journal of statistical planning and inference, vol. 43, no. 3,pp. 381–402, 1995.
[22] Julie. (2012) Surrogate model optimization toolbox, matlab central fileexchange. [Online]. Available: https://www.mathworks.com/matlabcen-tral/fileexchange/ 38530-surrogate-model -optimization-toolbox
[23] T. Wiens. (2014) Radial basis function network. [Online]. Available: https://www.mathworks.com/ matlabcentral/ fileexchange/ 22173-radial-basis-function-network
[24] EPSRC. (2021) Epsrc centre for doctoral training in fluid dynamics at leeds. [Online]. Available: https:// gow. epsrc. ukri.org/NGBOViewGrant.aspx?GrantRef=EP/L01615X/1